

# Eulerian spatio-temporal correlations in passive scalar turbulence

Anastasiia Gorbunova,<sup>1,2</sup> Carlo Pagani,<sup>1</sup> Guillaume Balarac,<sup>2,3</sup> Léonie Canet,<sup>1,3,\*</sup> and Vincent Rossetto<sup>1</sup>

<sup>1</sup>University Grenoble Alpes, CNRS, LPMMC, 38000 Grenoble, France

<sup>2</sup>University Grenoble Alpes, CNRS, Grenoble INP, LEGI, 38000 Grenoble, France

<sup>3</sup>Institut Universitaire de France, 1 rue Descartes, 75000 Paris, France

We study the spatio-temporal two-point correlation function of passively advected scalar fields in the inertial-convective range in three dimensions by means of numerical simulations. We show that at small time delays  $t$  the correlations decay as a Gaussian in the variable  $tp$  where  $p$  is the wavenumber. At large time delays, a crossover to an exponential decay in  $tp^2$  is expected from a recent functional renormalization group (FRG) analysis. We study this regime for a scalar field advected by a Kraichnan’s “synthetic” velocity field, and accurately confirm the FRG result, including the form of the prefactor in the exponential. By introducing finite time correlations in the synthetic velocity field, we uncover the crossover between the two regimes.

The advection of a scalar field by a turbulent flow plays a crucial role in several domains ranging from engineering to geophysics. For instance, a scalar field can represent the concentration of a chemically inactive impurity, or a temperature fluctuation. It is coined as passive when its backreaction on the flow is negligible. We focus on passive scalar fields in the inertial-convective range, which spans between the large scale at which the energy is injected and the small scale at which the dissipation occurs. In this range, the turbulent flow and the advected scalar both conform to the Richardson’s cascade picture, characterized by a constant downscale energy flux. In seminal works, Obukhov and Corrsin [1, 2] established that the 3D energy spectrum of the scalar field in this range decays as  $E_\theta(\vec{p}) \sim p^{-5/3}$ , hence exhibiting the same scaling as the one predicted by Kolmogorov in his 1941 statistical theory of turbulence [3, 4].

Despite much understanding has been gained on the statistical properties of scalars in fluid flows [4–7], certain aspects remain elusive. In particular, the time dependence of Eulerian correlation functions of a passive scalar field in a turbulent steady state is poorly understood. Its comprehension is essential for various applications, such as the development of time-accurate numerical models [9], experimental data treatment [10] and turbulent diffusion problems [11]. In early works [12, 13], it was suggested that the temporal properties of Eulerian correlation functions are determined by the random sweeping effect, i.e., the advection of small-scale velocities by random large-scale motion, which leads to a scaling of the correlation time as  $p^{-1}$ . Although the dominance of the sweeping effect has been discussed on phenomenological bases and observed in numerical simulations [14–16] and experiments [10], a more rigorous theoretical justification was missing.

Significant advances were provided by the analysis of simplified models of scalar turbulence, such as the model proposed by Kraichnan [17], in which the Navier-Stokes (NS) velocity field is replaced by a random vector field with a white-in-time Gaussian statistics. In suitable limits, this simplification indeed allows for explicit analyt-

ical calculations of the anomalous scaling exponents of the structure functions via different approaches [18–26], we refer to [4, 7, 27] for reviews. Furthermore, the temporal dependence of the scalar correlation function was analyzed in [28, 29]. However, the simplified velocity covariance prevents one from relating the model to real scalar turbulence.

Recently, the study of the temporal properties of correlation functions in a turbulent steady-state has received a boost triggered by the use of functional renormalization group (FRG) [30]. For NS turbulence, this framework allows one to obtain an analytical expression for arbitrary correlation functions in the limit of large wavenumbers. This arises from the fact that the FRG flow equations for these objects can be closed in a large wavenumber expansion exploiting only the symmetries and the related Ward identities [31–33]. Remarkably, within the FRG framework, one can derive an approximated form of the spatio-temporal Eulerian two-point correlation function of the scalar field advected by NS flows and in Kraichnan’s model [34].

In this Letter, we study scalar fields advected by NS flows as well as synthetic velocity fields in three dimensions by means of direct numerical simulations (DNS). We focus on the spatio-temporal dependence of the Eulerian two-point correlation function of the scalar field. We find that it exhibits two distinct time regimes in the stationary state: a Gaussian decay in the variable  $tp$  at small time differences  $t$  followed by an exponential decay in  $tp^2$  at large time differences, although the latter is only evidenced for the synthetic velocity field. Beyond the general form of the correlations, we also compute the non-universal prefactors in the exponentials, and show that these results are in accurate agreement with the FRG predictions, thereby providing a detailed and precise account of the Eulerian temporal behavior of scalar turbulence.

*Dynamics of the passive scalar field.* We consider a scalar field  $\theta(t, \vec{x})$  governed by the following advection-

diffusion equation

$$\partial_t \theta + v^j \partial_j \theta = \kappa \partial^2 \theta + f_\theta, \quad (1)$$

where  $\kappa$  is the molecular diffusivity and  $f_\theta$  a stochastic forcing peaked at some large scale  $L$ . The advection field  $\vec{v}(t, \vec{x})$  is the velocity of an incompressible fluid satisfying the NS equation,

$$\partial_t v^i + v^j \partial_j v^i = -\frac{1}{\rho} \partial_i \pi + \nu \partial^2 v^i + f^i, \quad (2)$$

where  $\pi$  denotes the pressure,  $\rho$  the density,  $\nu$  the viscosity, and  $f^i$  a stochastic forcing which injects energy at the same integral scale  $L$ . The scalar is assumed to be passive, which means that it does not affect the carrier fluid.

We also consider Kraichnan's model [17], in which the velocity is a random Gaussian vector field, characterized by zero mean and covariance

$$\langle v^i(t, \vec{x}) v^j(t', \vec{y}) \rangle = \delta(t - t') D_0 \int_{\vec{p}} \frac{e^{i\vec{p} \cdot (\vec{x} - \vec{y})} P_{ij}(\vec{p})}{(p^2 + m^2)^{\frac{d}{2} + \frac{\varepsilon}{2}}} \quad (3)$$

where  $P_{ij}(\vec{p}) \equiv \delta_{ij} - \frac{p_i p_j}{p^2}$  is the transverse projector which ensures incompressibility and  $\int_{\vec{p}} \equiv \int d^d \vec{p}$ . The parameter  $0 < \varepsilon/2 < 1$  corresponds to the Hölder exponent, describing the velocity roughness from very rough for  $\varepsilon \rightarrow 0$  to smooth for  $\varepsilon \rightarrow 2$ , and  $m$  acts as an IR cutoff.

*Theoretical results from FRG.* The FRG is a modern and versatile implementation of the Wilsonian RG [30]. Within this formalism, a generic  $n$ -point correlation function is calculated by deriving an equation governing its dependence on the RG scale, and solving it via some approximation scheme. For scalar turbulence, it turns out that the flow equation of the two-point function can be closed for large wavenumbers, thanks to the symmetries of the field theory associated to Eqs. (1) and (2) [34]. No additional approximation is needed besides the large wavenumber limit, in particular these results do not rely on any small expansion parameter, and this closure can be achieved for scalars advected by NS flows, as well as for Kraichnan's model.

In the case of NS flows, the FRG yields for the two-point correlation function  $C(t, \vec{p}) \equiv \langle \theta(t, \vec{p}) \theta(0, -\vec{p}) \rangle$  the following result

$$C(t, \vec{p}) = \frac{\epsilon_\theta \epsilon^{-1/3}}{p^{11/3}} \begin{cases} C_s \exp\left(-\alpha_s \frac{L^2}{\tau_0^2} p^2 t^2\right), & t \ll \tau_0 \\ C_\ell \exp\left(-\alpha_\ell \frac{L^2}{\tau_0} p^2 |t|\right), & t \gg \tau_0 \end{cases} \quad (4)$$

where  $\epsilon$  and  $\epsilon_\theta$  are the energy dissipation rates of the velocity and scalar fields respectively, and  $\tau_0 \equiv (L^2/\epsilon)^{-1/3}$  denotes the eddy-turnover time at the energy injection scale, we refer to [34] for details. The constants  $C_{s,\ell}$  and  $\alpha_{s,\ell}$  are not universal. Remarkably, the scalar field inherits in this range the temporal properties of the NS

velocity field, which exhibits a fully analogous behavior [31, 32]. The short time regime is known to be related to the random sweeping effect, while the long time regime was not identified before, but can also be simply interpreted on phenomenological grounds (see below). For NS velocity, the short time Gaussian decay of the two-point and three-point correlation functions was accurately confirmed by DNS [31, 35]. However, the large time exponential regime has remained elusive so far in the numerical simulations. Nevertheless, it can be accessed for the scalar field in the synthetic flow by tailoring the velocity covariance, as we show in the following.

For Kraichnan's model, due to the white-in-time nature of the velocity covariance, the FRG leads to an exponential time decay of the scalar correlation function for all times  $t$  as

$$C_K(t, \vec{p}) = F(p) e^{-\kappa_{\text{ren}} p^2 |t|} \quad (5)$$

where  $F(p)$  is a complicated integral. In the inertial range, one finds  $F(p) \sim p^{-d-2+\varepsilon}$  while in the weakly non-linear regime (i.e., when the convective term is perturbative),  $F(p) \sim p^{-d-2-\varepsilon}$  [34]. Moreover, one obtains an explicit expression for the renormalized diffusivity

$$\kappa_{\text{ren}} = \kappa + \frac{d-1}{2d} \int_{\vec{p}} \frac{D_0}{(p^2 + m^2)^{\frac{d}{2} + \frac{\varepsilon}{2}}}. \quad (6)$$

Remarkably, the temporal dependence in Eq. (5) can be derived via several approaches, both standard resummation of the self-energy diagrams and FRG calculation [34]. An analogous expression was obtained in [28, 29] by deriving a differential equation for the two-point correlation function.

The FRG approach allows one to go beyond the strict white-in-time limit of Kraichnan's model. One finds that as soon as the covariance (3) deviates from pure white noise, the two-point correlation function  $C_K(t, \vec{p})$  also develops a short time Gaussian regime, which is studied numerically in the following.

An intuitive interpretation of the short- and large-time regimes of the Eulerian spatio-temporal correlation function can be drawn from the single particle turbulent dispersion, as shown in Ref. [35]. In this picture, the arguments of the exponentials in Eq. (4) are related to the mean square displacement of a fluid particle, which is proportional to  $t^2$  (ballistic regime) at times at which the velocity field is correlated, while at large times, when the velocity is uncorrelated, it grows linearly in time [36], with a coefficient proportional to the eddy diffusivity.

*Direct numerical simulations (DNS).* To study the spatio-temporal correlation function of a passive scalar, we perform DNS of 3D homogeneous isotropic turbulent flows. The equations (1) and (2) are solved on a discrete cubic grid with the use of a pseudo-spectral method [1]. Further details on the DNS, snapshots of the velocity and scalar fields and their spatial spectra are provided in

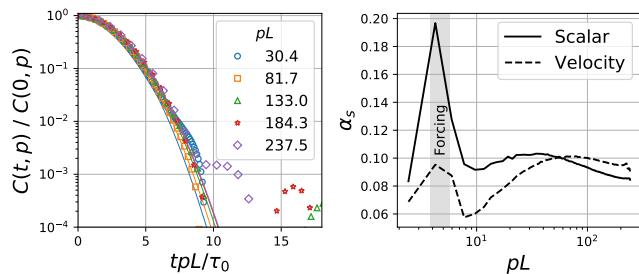


FIG. 1. *Left panel:* Normalized averaged two-point correlation function  $C(t, \vec{p})$  of the scalar field in the NS velocity field at various wavenumbers  $p$ , points are the numerical data and plain lines their Gaussian fits. All curves collapse when plotted against  $tp$  variable. *Right panel:* Dependence on the wavenumber  $p$  of the numerically estimated parameter  $\alpha_s$  for scalar and velocity. The Taylor Reynolds is number  $R_\lambda = 90$ , the Schmidt number  $Sc = 0.7$ . In all figures, the wavenumbers are non-dimensionalized by the integral scale  $L$ , and the times by  $\tau_0 = L/U_{\text{rms}}$  with  $U_{\text{rms}}$  the root mean square velocity.

[38]. Once the stationary state is reached, the two-point correlation function  $C(t, \vec{p})$  is calculated in spectral domain and averaged over time and wavenumber shells as described in [38].

*Scalar fields advected by NS flows.* For scalar fields in the inertial-convective range, we expect different behaviors at short and large time delays according to Eq. (4). In the short time regime, we find that the correlation functions obtained from the DNS all behave as a Gaussian. Their time dependence at fixed wavenumbers  $p$  is fitted with the two-parameter function  $g(t) = C_0 \exp[-at^2]$ . As illustrated in Fig. 1 (left panel), all curves collapse onto a single Gaussian when plotted as a function of the variable  $tp$ , as predicted by Eq. (4). The value of the fitting parameter  $a$  provides a numerical estimation of the decorrelation parameter  $\alpha_s$  in Eq. (4) as  $\alpha_s = a(\tau_0/Lp)^2$ . The dependence of the estimated parameter  $\alpha_s$  on the wavenumber is displayed in the right panel of Fig. 1, showing that both velocity and scalar reach a plateau beyond the forcing range, in agreement with the short-time expression in Eq. (4). Moreover, the numerical values of  $\alpha_s$  for the scalar and velocity fields are very close, which is also in agreement with the FRG result, predicting that  $\alpha_s$  is solely determined by the properties of the carrier flow and is the same for the velocity and for the scalar. Besides, this result demonstrates that the typical decorrelation time scales as  $a^{-1/2} \sim p^{-1}$ , thus, the Eulerian spatio-temporal correlations are dominated by the sweeping effect.

At large time delays  $t$ , one expects a crossover to an exponential decay in time according to Eq. (4). In the DNS, the correlations become very small and oscillatory after the Gaussian decay, preventing the direct observation of this crossover. However, it can be uncovered in a

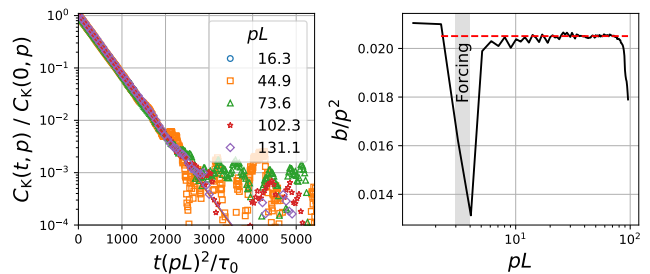


FIG. 2. *Left panel:* Two-point correlation function  $C_K(t, \vec{p})$  at various wavenumbers  $p$  of a passive scalar in 3D DNS of Kraichnan's random advection model for  $\varepsilon = 1$ . All curves collapse onto a single exponential when plotted against the variable  $tp^2$ . *Right panel:* dependence of the ratio  $b/p^2$  on the wavenumber. The dashed line corresponds to the plateau value.

synthetic flow, as we now discuss.

*Scalar fields in Kraichnan's model.* We perform several sets of simulations, where the velocity field is artificially generated and tailored to have a Gaussian statistics. The velocity covariance is

$$\langle \hat{v}_i(t_0 + t, \vec{p}) \hat{v}_j^*(t_0, \vec{p}) \rangle = \frac{D_0}{T_e} (p^2 + m^2)^{-\frac{3-\varepsilon}{2}} P_{ij}(\vec{p}) \quad (7)$$

for  $0 < t < T_e$  and vanishes otherwise, with  $T_e = n\Delta t$ , where  $\Delta t$  is the simulation time step and  $n$  the number of iterations before the velocity is updated. The velocity field is generated in Fourier space and fulfills the prescribed spatial covariance, as well as the conditions of isotropy and zero divergence. For  $T_e$  small compared to the dynamical time scales of the flow ( $\tau_A \sim \Delta x/U_{\text{rms}}$  for advection, and  $\tau_\kappa \sim (\Delta x)^2/\kappa$  for diffusion, with  $\Delta x$  spatial grid cell), the velocity field can be considered as white-in-time.

We analyze 4 sets of simulations allowing to describe the various regimes by changing the Hölder exponent and the amplitude of the velocity covariance, as well as the scalar diffusivity. Set 1 corresponds to the inertial regime, set 2 to the weakly non-linear regime, sets 3 and 4 to transitional regimes. All parameters are provided in [38]. We first note that the equal-time two-point scalar correlation functions show a remarkable agreement with the expected power laws for both the inertial and the weakly non-linear regime [38].

At unequal times, the two-point spatio-temporal correlation function was measured numerically for all sets. We find that the time dependence of  $C_K(t, \vec{p})/C_K(0, \vec{p})$  at fixed wavenumbers is always an exponential, as illustrated in Fig. 2 (left panel). Moreover, when plotted as a function of  $tp^2$ , all the curves collapse onto a single exponential. Furthermore, we fitted all curves with the two-parameter function  $g_K(t) = C_0 \exp[-bt]$ . The right panel of Fig. 2 shows that the fitting parameter  $b$  compensated by  $p^2$  takes an approximately constant value in

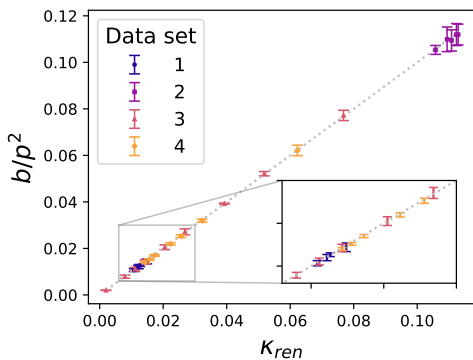


FIG. 3. Renormalized scalar diffusivity  $\kappa_{\text{ren}}$  obtained as the decorrelation parameter  $b/p^2$  of the exponential fit of the scalar correlation function versus its theoretical estimate based on the Eq. (6) for our 4 data sets (see [38] for detailed parameters). The error bars correspond to doubled standard deviation of  $b/p^2$  from the estimated plateau value, as shown in the right panel of Fig. 2.

a large range of wavenumbers, demonstrating that the correlation functions  $C_K(t, \vec{p})$  indeed take the expected form (5).

In the exponential, the prefactor  $\kappa_{\text{ren}}$  depends on the details of the velocity statistics and cutoffs. In order to make a precision test of its expression, we varied the amplitude  $D_0$ , the diffusivity  $\kappa$ , and Hölder exponent through our 4 sets.

The plateau value of the ratio  $b/p^2$  gives a numerical estimate of the renormalized diffusivity  $\kappa_{\text{ren}}$  in Eq. (5). Besides, the expression for  $\kappa_{\text{ren}}$  given by Eq. (6) can be estimated in the simulations upon replacing the integral over wavenumbers by a sum over discrete modes. The value of  $(\kappa_{\text{ren}} - \kappa)$  is fixed by the velocity properties only, and can be computed without any information about the scalar. In Fig. 3, we show the comparison between the value of  $\kappa_{\text{ren}}$  computed via the correlation fit and via the theoretical expression. We obtain a remarkable agreement for all four data sets, thus demonstrating that the temporal dependence in Eq. (5) is valid for all regimes, even though the equal-time part  $F(p)$  behaves differently. Let us emphasize that the obtained results are tested for values of  $\varepsilon$  spanning up to 1.5, well beyond the perturbative regime [23]. This analysis hence provides a thorough confirmation of the theory, up to the precise form of the prefactor in the exponential.

*Crossover between the short- and large-time regimes.* We perform a simulation with a larger renewal time period  $T_e$  of the velocity field, during which the scalar is evolving in a “frozen” velocity field. Clearly, the white-in-time approximation breaks down in this case. The temporal correlations of the velocity field alters the small-time behavior of the scalar, which is then expected to decay as a Gaussian in  $tp$ , similarly to the scalar in the NS flow. We show in Fig. 4 (inset) the correlation function of

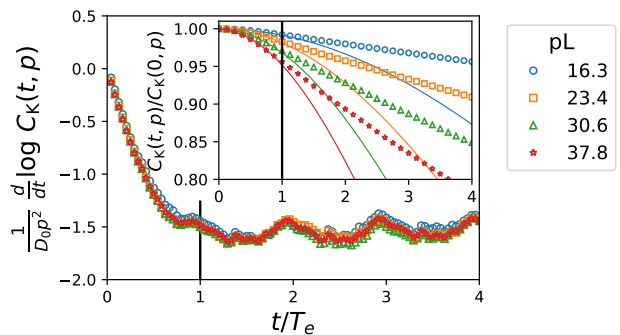


FIG. 4. Scalar correlation  $C_K(t, \vec{p})$  (inset) at time scales comparable to the velocity field renewal period  $T_e$  for various wavenumbers  $p$ . The continuous lines correspond to the Gaussian fit of the points at  $t < T_e$ . The main panel shows the time derivative of  $\log C_K(t, \vec{p})$ . The linear part at  $t < T_e$  corresponds to the Gaussian time decay, while the nearly constant part at  $t > T_e$  corresponds to an exponential time dependence. The curves at various wavenumbers are rescaled vertically by  $p^2$  which leads to their collapse.

a passive scalar in a random velocity field updated every  $n = 24$  iterations. We found that at times  $t < T_e$  its correlation function  $C_K(t, \vec{p})$  behaves as a Gaussian, while at  $t > T_e$ , the correlation curves significantly deviate from the Gaussian and endow an exponential form, similar to the ones in Fig. 2. The transition between the small- and large-time decays can be visualized by analyzing the time derivative of  $\log C_K(t, \vec{p})$ . When  $C_K(t, \vec{p})$  is a Gaussian, this derivative decreases linearly, whereas when  $C_K(t, \vec{p})$  is an exponential, it is a negative constant. In Fig. 4, we show that the derivative of  $\log C_K(t, \vec{p})$  exhibits the expected crossover from a linear decay to a constant. In addition, the rescaling of the derivatives by  $1/p^2$  leads to a collapse of all curves, demonstrating that the Gaussian and the exponential both possess a  $p^2$ -dependence on the wavenumber, as expected from Eq. (4).

At high wavenumbers, the large-time regime becomes indiscernible as the scalar field decorrelates fast (because of the  $\sim p^2$  dependence) down to near-zero values. We believe that a similar effect hinders the large-time regime in NS flows.

*Summary and future prospects.* Our work shows that the two-point Eulerian spatio-temporal correlation function of a passive scalar in a 3D homogeneous isotropic turbulent takes a Gaussian form in the variable  $pt$  at short time delays  $t$ . In addition, the coefficient characterizing the Gaussian time decay of the scalar field is approximately the same as the one of the velocity field. According to the FRG prediction, the two-point correlation function possesses a large-time regime, as displayed in Eq. (4). In order to study the crossover between the two regimes, we analyzed the time correlations of a scalar advected by a synthetic velocity field. We observe that in the case of white-in-time velocity covariance, the correla-

tion function accurately follows the expected exponential decay in  $p^2t$ , including the precise form of the prefactor of the exponential. Moreover, switching from a white-in-time to a non-trivial time covariance of the synthetic velocity field allows one to reveal the crossover between the two time regimes. These results thus confirm the predictions of the FRG analysis and provide hints that a similar crossover should be present also in the case of scalar fields advected by NS flows, although it could not be detected in our simulations. It would be very interesting to extend this analysis to higher-order correlation functions. We believe that the case of non-passive scalars could also be studied using similar methods.

This work was supported by ANR-18-CE92-0019 Grant NeqFluids. L.C. and G.B. acknowledge support from Institut Universitaire de France. The simulations were performed using the high performance computing resources from GENCI-IDRIS (grant 020611) and the GRICAD infrastructure (<https://gricad.univ-grenoble-alpes.fr>), which is supported by Grenoble research communities.

---

\* leonie.canet@grenoble.cnrs.fr

- [1] A. M. Obukhov, *Izv. Geogr. Geophys.* **13**, 58 (1949).
- [2] S. Corrsin, *J. Appl. Phys.* **22**, 469 (1951).
- [3] A. N. Kolmogorov, *C.R. Acad. Sci. URSS* **30**, 301 (1941).
- [4] A. N. Kolmogorov, *Dokl. Akad. Nauk SSSR* **30**, 299 (1941).
- [5] K. R. Sreenivasan, *PNAS* **116**, 18175 (2019).
- [6] Z. Warhaft, *Annu. Rev. Fluid Mech.* **32**, 203 (2000).
- [7] B. I. Shraiman and E. D. Siggia, *Nature* **405**, 639 (2000).
- [4] G. Falkovich, K. Gawędzki, and M. Vergassola, *Rev. Mod. Phys.* **73**, 913 (2001), arXiv:cond-mat/0105199.
- [9] G. He, G. Jin, and Y. Yang, *Annu. Rev. Fluid Mech.* **49**, 51 (2017).
- [10] X. He and P. Tong, *Phys. Rev. E* **83**, 037302 (2011).
- [11] A. J. Majda and P. R. Kramer, *Phys. Rep.* **314**, 237 (1999).
- [12] R. H. Kraichnan, *Phys. Fluids* **7**, 1723 (1964).
- [13] H. Tennekes, *J. Fluid Mech.* **67**, 561 (1975).
- [14] S. Chen and R. H. Kraichnan, *Phys. Fluids A: Fluid Dyn.* **1**, 2019 (1989).
- [15] P. K. Yeung and B. L. Sawford, *J. Fluid Mech.* **459**, 129 (2002).
- [16] P. A. O’Gorman and D. I. Pullin, *J. of Turbulence* **5**, N35 (2004).
- [17] R. H. Kraichnan, *Phys. Fluids* **11**, 945 (1968).
- [18] M. Chertkov and G. Falkovich, *Phys. Rev. Lett.* **76**, 2706 (1996).
- [19] M. Chertkov, G. Falkovich, I. Kolokolov, and V. Lebedev, *Phys. Rev. E* **52**, 4924 (1995).
- [20] K. Gawędzki and A. Kupiainen, *Phys. Rev. Lett.* **75**, 3834 (1995), arXiv:chao-dyn/9506010.
- [21] D. Bernard, K. Gawędzki, and A. Kupiainen, *Phys. Rev. E* **54**, 2564 (1996), arXiv:chao-dyn/9601018.
- [22] D. Bernard, K. Gawędzki, and A. Kupiainen, *Journal of Statistical Physics* **90**, 519 (1998), arXiv:cond-mat/9706035.
- [23] L. T. Adzhemyan, N. V. Antonov, and A. N. Vasil’ev, *Phys. Rev. E* **58**, 1823 (1998).
- [24] L. T. Adzhemyan, N. V. Antonov, V. A. Barinov, Y. S. Kabrits, and A. N. Vasil’ev, *Phys. Rev. E* **63**, 025303 (2001).
- [25] A. Kupiainen and P. Muratore-Ginanneschi, *J. Statist. Phys.* **126**, 669 (2007), arXiv:nlin/0603031.
- [26] C. Pagani, *Phys. Rev. E* **92**, 033016 (2015), [Addendum: *Phys.Rev.E* **97**, 049902 (2018)].
- [27] N. V. Antonov, *J. Phys. A: Math. Gen.* **39**, 7825 (2006).
- [28] D. Mitra and R. Pandit, *Phys. Rev. Lett.* **95**, 144501 (2005).
- [29] S. Sankar Ray, D. Mitra, and R. Pandit, *New J. Phys.* **10**, 033003 (2008).
- [30] N. Dupuis, L. Canet, A. Eichhorn, W. Metzner, J. M. Pawłowski, M. Tissier, and N. Wschebor, *Phys. Rep.* (2021), 10.1016/j.physrep.2021.01.001.
- [31] L. Canet, V. Rossetto, N. Wschebor, and G. Balarac, *Phys. Rev. E* **95**, 023107 (2017).
- [32] M. Tarpin, L. Canet, and N. Wschebor, *Phys. Fluids* **30**, 055102 (2018).
- [33] M. Tarpin, L. Canet, C. Pagani, and N. Wschebor, *J. Phys. A: Math. Theor.* **52**, 085501 (2019).
- [34] C. Pagani and L. Canet, (2021), arXiv:2103.07326 [cond-mat, physics:physics].
- [35] A. Gorbunova, G. Balarac, L. Canet, G. Eyink, and V. Rossetto, *Phys. Fluids* **33**, 045114 (2021), arXiv:2102.02858.
- [36] G. I. Taylor, *Proc. London Math. Soc.* **s2-20**, 196 (1922).
- [1] C. Canuto, ed., *Spectral Methods: Evolution to Complex Geometries and Applications to Fluid Dynamics*, Scientific Computation (Springer, Berlin ; New York, 2007).
- [38] See Supplemental Material at [URL will be inserted by publisher] for detailed parameters, spectra and field snapshots of simulations.

## Appendix

In this appendix, we provide the detailed description of the simulations performed to obtain the data analyzed in the main text, as well as additional figures of the velocity and scalar fields and their spatial spectra.

### SIMULATIONS OF SCALAR ADVECTION IN NAVIER-STOKES VELOCITY FIELD

The direct numerical simulations (DNS) of the Navier-Stokes equation for the turbulent velocity field and advection-diffusion equation for the passive scalar are performed in a three-dimensional periodic cubic domain of size  $2\pi$ , with different resolutions, Reynolds and Péclet numbers (see Table I). The equations are solved on a discrete grid with the use of a pseudo-spectral method in space and the second order Runge-Kutta scheme for time advancement [1]. The spatial resolution of the velocity is determined by the condition  $p_{max}\eta = 1.5$ , where  $p_{max}$  is the maximal wavenumber in the computational domain,  $\eta$  is the Kolmogorov length scale. Dealiasing errors are reduced by the polyhedral truncation method [2]. In order to reach a statistically stationary state of the flow, both the velocity and the passive scalar fields are forced randomly in spectral space at large scales [3]. The random forcing field is independent from the velocity and scalar and is updated at each time step of the simulation. This forcing scheme yields a numerical approximation of the stochastic forcing, which is also assumed to be white-in-time. An example of instantaneous 2D snapshots of the velocity and scalar fields is displayed in the Fig. 5, for the spatial resolution  $N^3 = 256^3$ , the Taylor-scale Reynolds number  $R_\lambda = 90$  and the Schmidt number  $Sc = 0.7$ . We show in Fig. 6 the corresponding kinetic energy spectrum of the Navier-Stokes velocity field and the spectrum of variance of the scalar field. The spectra are averaged in time once the stationary state is reached.

$R_\lambda$	$N_v$	$Sc$	$N_s$	$Pe$	$\Delta t/\tau_0$	$\Delta T_w/\tau_0$	$N_w$
60	128	0.7	128	222	$1.4 \times 10^{-3}$	0.7	795
60	128	16	512	5088	$3.5 \times 10^{-5}$	0.07	21
60	128	36	768	11448	$2.1 \times 10^{-5}$	0.03	16
90	256	0.7	256	931	$1.1 \times 10^{-4}$	2.94	50

TABLE I. Parameters of DNS of scalar advection in Navier-Stokes velocity field.  $R_\lambda$  - Taylor-scale Reynolds number,  $N_s$  - spatial grid resolution for velocity,  $Sc$  - scalar Schmidt number,  $N_s$  - spatial grid resolution for scalar,  $Pe$  - Péclet number,  $\tau_0$  - large-scale eddy-turnover time,  $\Delta t$  - simulation time step,  $\Delta T_w$  - width of a time window of correlation measurement,  $N_w$  - number of recorded time windows for time correlation.

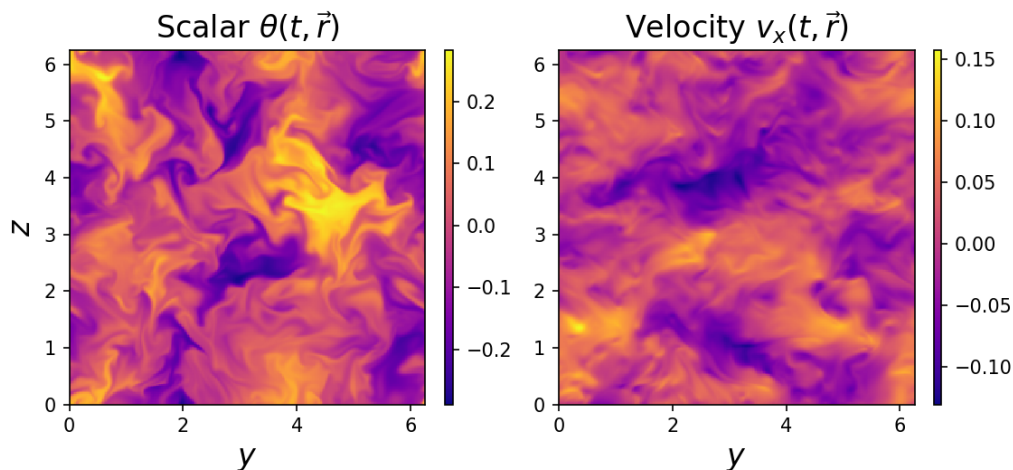


FIG. 5. Instantaneous 2D snapshots of the scalar field and of the  $x$ -component of the velocity field, obtained from the DNS of the Navier-Stokes equation at Taylor-scale Reynolds number  $R_\lambda = 90$  on a grid of size  $N^3 = 256^3$ , with the Schmidt number of the scalar  $Sc = 0.7$ .

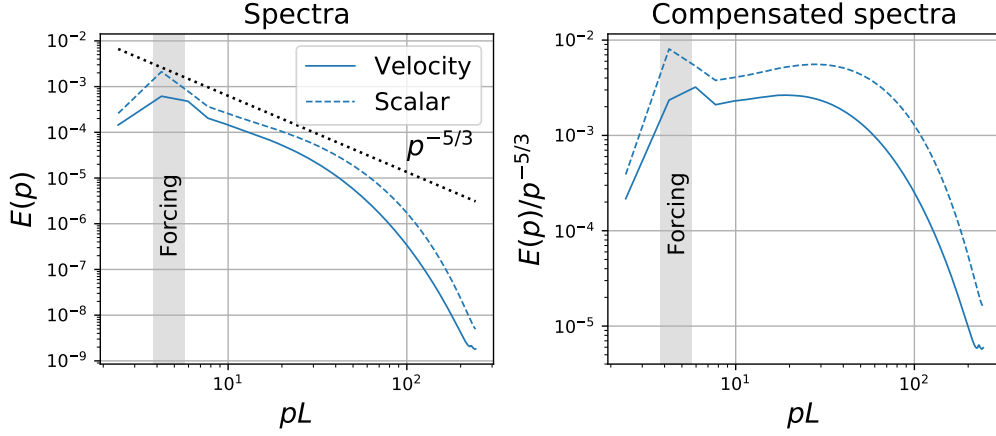


FIG. 6. Spectra and compensated spectra of the velocity kinetic energy and scalar variance from DNS at Taylor-scale Reynolds number  $R_\lambda = 90$  on a grid of size  $N^3 = 256^3$ , with the Schmidt number of the scalar  $Sc = 0.7$ .

The correlation function of the scalar field is also computed in the stationary state, and is averaged in time and in space, over spherical spectral shells  $S_n$  of thickness  $\Delta p = 1$ , which can be written as:

$$C(t, \vec{p}) = \frac{1}{N_t} \sum_{j=1}^{N_t} \frac{1}{M_n} \sum_{\vec{p} \in S_n} \text{Re} [\theta(t_{0j}, \vec{p}) \theta^*(t_{0j} + t, \vec{p})], \quad (8)$$

where  $N_t$  is the number of time windows in the simulation, and  $M_n$  is the number of modes in the spectral spherical shell  $S_n$ . The same computation was simultaneously performed for the velocity correlations.

### SIMULATIONS OF SCALAR ADVECTION IN SYNTHETIC VELOCITY FIELD

To approximate the stochastic white-in-time self-similar velocity field of the Kraichnan model of passive scalar transport, we implemented a synthetic field generator which realizes the following variance:

$$\langle \hat{u}_i(t_0, \vec{p}) \hat{u}_j^*(t_0 + t, \vec{p}) \rangle = \begin{cases} \frac{D_0}{T_e} (p^2 + m^2)^{-\frac{3-\varepsilon}{2}} P_{ij}(\vec{p}) & t < T_e \\ 0 & t > T_e \end{cases}$$

$T_e$  thus represents the existence time of an individual realization of the velocity field, which is calculated as  $T_e = n\Delta t$ , where  $n$  is the number of time iterations before a new velocity field is generated. The infra-red cut-off wavenumber  $m$  is set to 1 in all simulations. When  $T_e$  is negligible compared to the other characteristic time scales of the flow, we obtain an approximation of the  $\delta$ -function in time.

The velocity field is generated in Fourier space in the following way:

$$\hat{u}(t, \vec{p}) = \sqrt{\frac{2D_0(p^2 + m^2)^{-\frac{3-\varepsilon}{2}}}{T_e}} \vec{\eta}(t, \vec{p}) \quad (9)$$

where  $\vec{\eta}$  is a unit random complex vector fulfilling the requirements of zero-divergence and isotropy. The velocity field can also be characterized by the root-mean-square velocity  $u_{RMS} = \sqrt{2E_k/3}$ , with  $E_k$  the total kinetic energy. It is linked with  $D_0$  by  $u_{RMS} = \sqrt{A \frac{D_0}{2T_e}}$ , where  $A = \frac{1}{3} \sum_{\vec{p}} (p^2 + m^2)^{-\frac{3-\varepsilon}{2}}$  is the constant coming from the numerical estimation of the integral of the spatial velocity spectrum. The random velocity field is generated in spectral space every  $n$  iterations and is totally uncorrelated with the previous realizations.

The scalar field is also subjected to a large-scale random forcing. The forcing term  $f_\theta$  is generated at each iteration in spectral space within a narrow wavenumber band  $3 < p_f < 4$  corresponding to large scales. The amplitude of the forcing is the same in all simulations. The dynamics of the scalar can be characterized by a non-dimensional parameter analogous to the Péclet number [4]  $Pe = D'_0 L^\varepsilon / \kappa$ , where  $D'_0 = D_0 / \varepsilon$ , and  $L$  corresponds to the scalar

integral length scale  $L = 2\pi/p_f$ . For each simulation the renormalized scalar diffusivity was estimated numerically according to Eq. (6) of the main text:

$$\kappa_{\text{ren}} = \kappa + \frac{1}{3} \sum_p \frac{D_0}{(p^2 + m^2)^{\frac{d}{2} + \frac{\varepsilon}{2}}} = \kappa + AD_0 \quad (10)$$

The parameters of all the simulations are provided in Table II. The simulations are divided into four sets. The sets 1 and 2 contain simulations at various  $\varepsilon$  with the parameter  $D_0$  kept constant. Low values of the parameter  $\varepsilon$  correspond to rough velocity fields, while higher  $\varepsilon$  values correspond to smoother ones. Instantaneous snapshots of the velocity fields at various  $\varepsilon$  are shown in Fig. 7. In the set 1 the diffusivities  $\kappa$  were chosen small ( $Pe > 1$ ) to reach the inertial regime, dominated by the advection. In the set 2 the diffusivity is fixed at a higher value, so that  $Pe \sim 0.1$ . In this case the scalar transport is dominated by diffusion but still affected by the advection. For this reason we refer to this regime as weakly non-linear. The snapshots of the scalar fields for the data sets 1 and 2 are provided in Figs. 8 and 9, respectively.

set	$N$	$\kappa$	$\varepsilon$	$D_0$	$n$	$\Delta t$	$U_{RMS}$	$Pe$	$A$	$N_w$	$\kappa_{\text{ren}}$
1	256	$6 \times 10^{-3}$	0.1	$4.18 \times 10^{-4}$	6	$0.24 \times 10^{-3}$	2.87	1.45	14.56	8	$1.22 \times 10^{-2}$
	256	$1.70 \times 10^{-3}$	0.5	$2.09 \times 10^{-3}$	6	$0.24 \times 10^{-3}$	4.22	6.54	6.28	10	$1.48 \times 10^{-2}$
	384	$1.7 \times 10^{-4}$	1.0	$4.18 \times 10^{-3}$	9	$0.16 \times 10^{-3}$	3.54	85.7	2.96	17	$1.25 \times 10^{-2}$
	384	$2.5 \times 10^{-5}$	1.5	$6.27 \times 10^{-3}$	9	$0.16 \times 10^{-3}$	3.32	793	1.72	17	$1.08 \times 10^{-2}$
2	192	0.1	0.1	$4.18 \times 10^{-4}$	6	$0.32 \times 10^{-3}$	2.42	0.09	13.81	26	$10.58 \times 10^{-2}$
	192	0.1	0.5	$2.09 \times 10^{-3}$	6	$0.32 \times 10^{-3}$	3.62	0.11	6.16	5	$11.29 \times 10^{-2}$
	192	0.1	1.0	$4.18 \times 10^{-3}$	6	$0.32 \times 10^{-3}$	3.55	0.15	2.96	5	$11.23 \times 10^{-2}$
	192	0.1	1.5	$6.27 \times 10^{-3}$	6	$0.32 \times 10^{-3}$	3.32	0.20	1.72	5	$11.08 \times 10^{-2}$
3	64	$2 \times 10^{-3}$	1.0	0.0	-	$0.98 \times 10^{-3}$	0.0	0.0	-	440	$2 \times 10^{-3}$
	64	$2 \times 10^{-3}$	1.0	$2.09 \times 10^{-3}$	2	$0.98 \times 10^{-3}$	2.86	2.5	2.86	440	$0.80 \times 10^{-2}$
	96	$2 \times 10^{-3}$	1.0	$3.14 \times 10^{-3}$	3	$0.65 \times 10^{-3}$	3.05	3.76	2.91	318	$1.11 \times 10^{-2}$
	128	$2 \times 10^{-3}$	1.0	$4.18 \times 10^{-3}$	4	$0.49 \times 10^{-3}$	3.23	5.02	2.93	266	$1.42 \times 10^{-2}$
	192	$2 \times 10^{-3}$	1.0	$6.28 \times 10^{-3}$	6	$0.32 \times 10^{-3}$	4.34	7.52	2.95	95	$2.05 \times 10^{-2}$
	256	$2 \times 10^{-3}$	1.0	$8.37 \times 10^{-3}$	8	$0.24 \times 10^{-3}$	5.03	10.04	2.97	49	$2.68 \times 10^{-2}$
	384	$2 \times 10^{-3}$	1.0	$12.55 \times 10^{-3}$	12	$0.16 \times 10^{-3}$	6.16	22.52	2.97	35	$3.92 \times 10^{-2}$
	512	$2 \times 10^{-3}$	1.0	$16.75 \times 10^{-3}$	16	$0.12 \times 10^{-3}$	7.12	30.03	2.98	35	$5.18 \times 10^{-2}$
768	$2 \times 10^{-3}$	1.0	$25.10 \times 10^{-3}$	32	$0.06 \times 10^{-3}$	8.74	45.05	2.98	39	$7.68 \times 10^{-2}$	
4		0.05						0.30			$6.22 \times 10^{-2}$
		0.02						0.75			$3.22 \times 10^{-2}$
	128	0.013	1.0	$8.36 \times 10^{-3}$	4	$0.49 \times 10^{-3}$	3.23	1.12	2.93	34	$2.56 \times 10^{-2}$
		0.01						1.50			$2.22 \times 10^{-2}$
		0.005						3.00			$1.72 \times 10^{-2}$
		0.0033						4.50			$1.56 \times 10^{-2}$
		0.002						7.51			$1.43 \times 10^{-2}$

TABLE II. Parameters of simulations of scalars in synthetic velocity fields.  $N$  - spatial resolution of the computational grid,  $\kappa$  - scalar diffusivity,  $\varepsilon$  - Hölder exponent of the velocity field,  $D_0$  - amplitude of the velocity covariance,  $n$  - number of iterations between velocity field updates,  $\Delta t$  - simulation time step,  $U_{RMS}$  - root-mean-square velocity,  $Pe$  - Péclet number,  $A$  - sum of the velocity spectrum,  $N_w$  - numbers of time windows for correlations averaging,  $\kappa_{\text{ren}}$  - numerical estimation of the renormalized diffusivity estimated according to Eq. (10)

We also generated two additional sets of data in order to test the dependence of  $\kappa_{\text{ren}}$  as given by Eq. 10 on the amplitude  $D_0$  of the velocity covariance and on the bare diffusivity  $\kappa$ . Thus, the set 3 consists of simulations at a fixed value of diffusivity  $\kappa$  and  $\varepsilon = 1$ , with gradually increasing the velocity covariance amplitude  $D_0$ . The first simulation at  $D_0 = 0$  corresponds to the purely diffusive case. The set 4 consists of a single simulation in which 7 scalars with various diffusivities are transported simultaneously by the same velocity field, with  $\varepsilon = 1$  and fixed  $D_0$ .

We show in the Fig. 10 the equal-time correlation functions for the velocity and the scalar field in the set 1, which is the inertial regime, and in the set 2, which is the weakly non-linear regime. The corresponding power-laws  $p^{-d-2+\varepsilon}$



and  $p^{-d-2-\varepsilon}$  respectively are accurately observed for all values of  $\varepsilon$ .

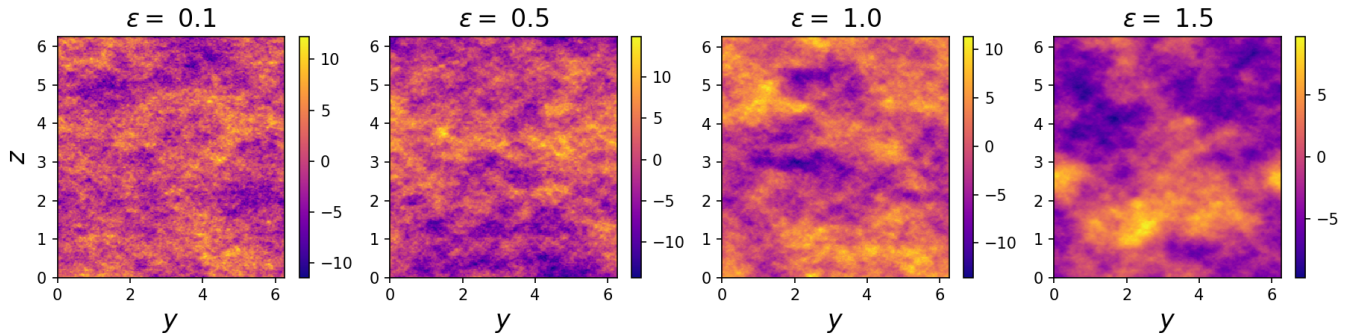


FIG. 7. Two-dimensional instantaneous cuts of the  $x$ -component of the synthetic velocity field at various  $\varepsilon$ .

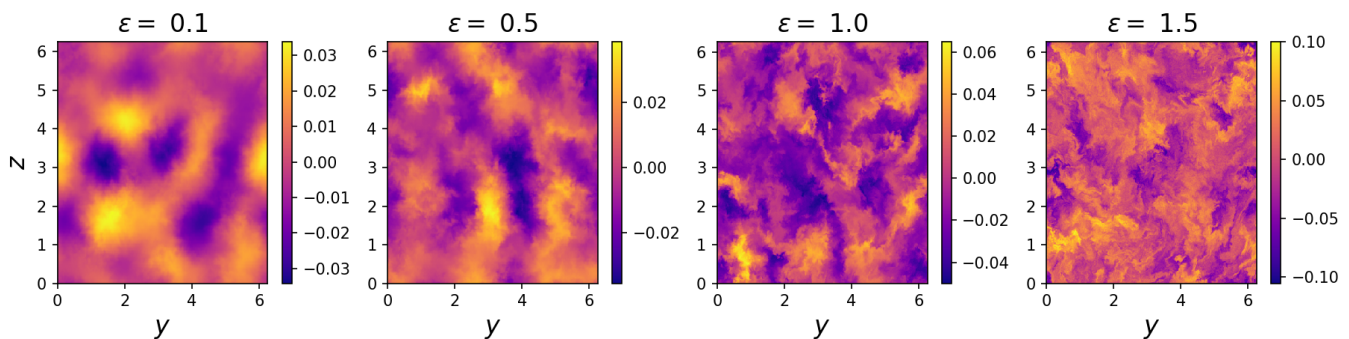


FIG. 8. Two-dimensional instantaneous cuts of the passive scalar field at various  $\varepsilon$  in the inertial regime (corresponding to set 1).

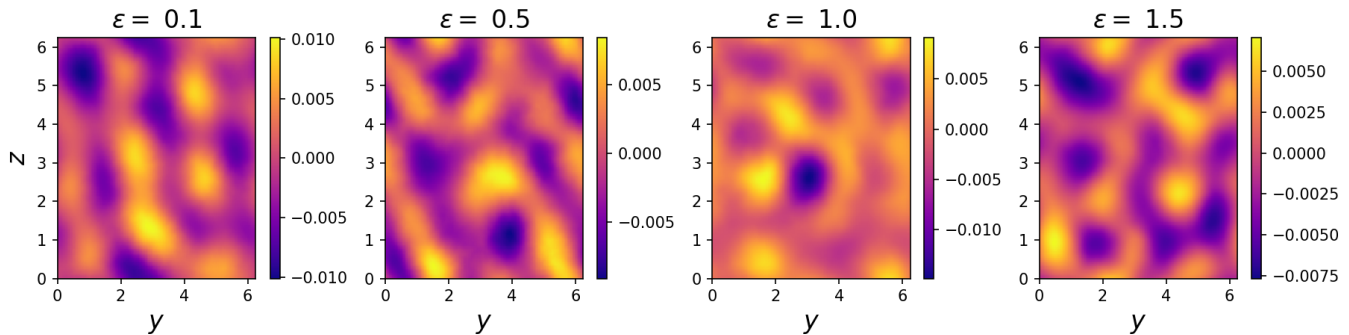


FIG. 9. Two-dimensional instantaneous cuts of the passive scalar field at various  $\varepsilon$  in the weakly non-linear regime (corresponding to set 2).

---

\* leonie.canet@grenoble.cnrs.fr

- [1] C. Canuto, ed., *Spectral Methods: Evolution to Complex Geometries and Applications to Fluid Dynamics*, Scientific Computation (Springer, Berlin ; New York, 2007).
- [2] S. A. Orszag, Numerical Simulation of Incompressible Flows Within Simple Boundaries. I. Galerkin (Spectral) Representations, *Studies in Applied Mathematics* **50**, 293 (1971).
- [3] K. Alvelius, Random forcing of three-dimensional homogeneous turbulence, *Physics of Fluids* **11**, 1880 (1999).

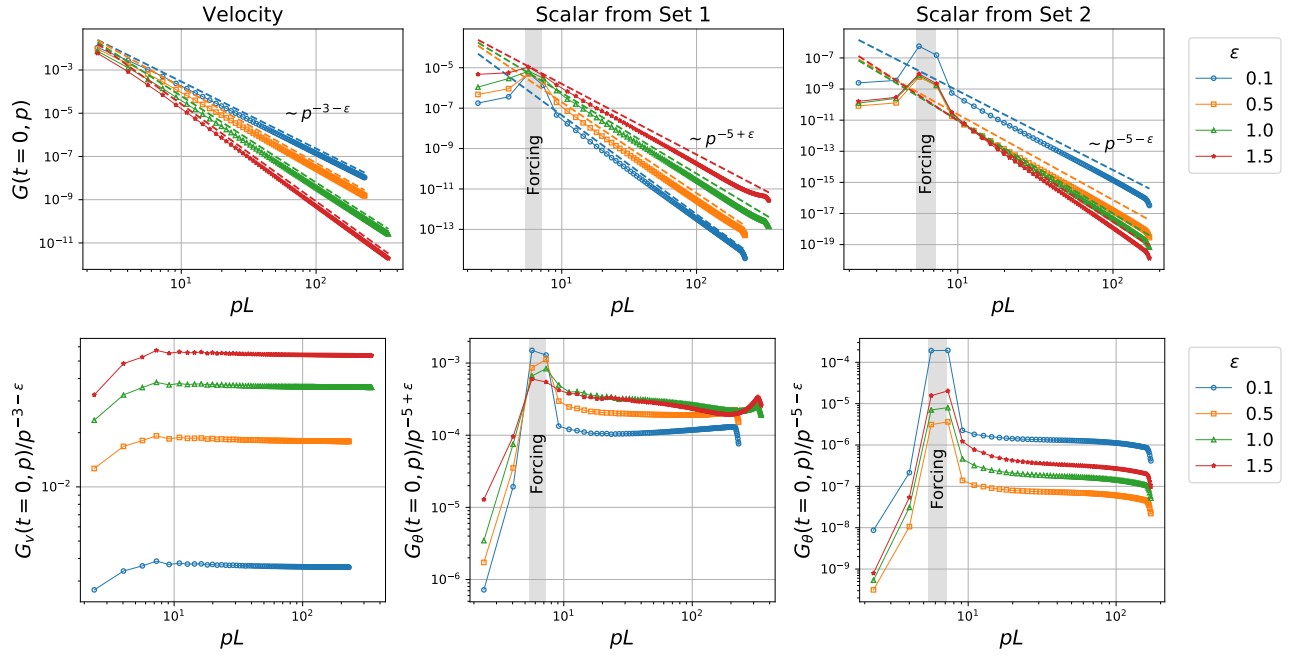


FIG. 10. Upper row: equal-time two-point correlation function of the velocity and scalars from data set 1 (inertial regime) and set 2 (weakly non-linear regime). Points correspond to the numerical data, the dashed lines to the corresponding theoretical power law. The bottom row show the same data but compensated by the theoretically predicted power law.

- [4] G. Falkovich, K. Gawędzki, and M. Vergassola, Particles and fields in fluid turbulence, *Reviews of Modern Physics* **73**, 913 (2001), arXiv:cond-mat/0105199.